PCCP

Accepted Manuscript

ROYAL SOCIETY OF CHEMISTRY

www.rsc.org/pccp

Journal Name

RSCPublishing

ARTICLE

Improving the Electrochemical Properties of $LiNi_{0.5}Co_{0.2}Mn_{0.3}O_2$ at 4.6 V Cutoff Potential by Surface Coating with Li_2TiO_3 for Lithium-ion Batteries

Cite this: DOI: 10.1039/x0xx00000x

Received 00th January 2012,
Accepted 00th January 2012

DOI: 10.1039/x0xx00000x

www.rsc.org/

Jing Wang,[a] Yangyang Yu,[a] Bing Li,[b] Tao Fu,[a] Dongquan Xie,[a] Jijun Cai[a] and Jinbao Zhao*[a,b]

The Li_2TiO_3-coated $LiNi_{0.5}Co_{0.2}Mn_{0.3}O_2$ (LTO@NCM) cathode materials are synthesized via *in situ* co-precipitation method followed by the lithiation process and thermal annealing. The Li_2TiO_3 coating layer is designed to strongly adhere to the core-material with 3D diffusion pathways for Li^+ ions. Electrochemical tests suggest that compared with pristine NCM, Li_2TiO_3 serves as both a Li ion conductive layer and protective coating layer against the attack from HF in electrolyte, and remarkably improves the cycling performance at higher charged state and rate capability of LTO@NCM composite material. What's more, phase transformation of NCM and metal ions dissolution at high-temperature at 4.6 V cutoff potential are effectively suppressed after LTO-coating. Our study demonstrates that LTO-coating on the surface of NCM is a viable method to improve the electrochemical performance of NCM, especially at high rates and high-voltage charged conditions.

Introduction

High performance rechargeable batteries are required to fulfill the rapidly growing demand for electric (EV), hybrid electric (HEV) and plug-in hybrid electric vehicles (PHEV). [1-6] Due to high voltage, high specific capacity and excellent cycling life and other advantages, lithium ion batteries (LIBs) are regarded as the most likely power source for electrical vehicles rather than the 'old-type' rechargeable batteries. [7, 8] Substantial researches have proved that the performance of lithium-ion batteries were mainly determined by the property of the cathode materials and thus great efforts have been made to optimize the cathode materials with high energy density. [9]

The primary approach to improve the energy density of battery is to develop cathode materials with high capacity [10] or/and higher operating voltages. [11] In this respect, layered nickel-rich oxide $LiNi_{0.5}Co_{0.2}Mn_{0.3}O_2$ is a competitive candidate owing to its low cost, low toxicity and high specific capacity compared with the mainstream commercial $LiCoO_2$. [12, 13] However, poor cycling performance and inferior thermal stability of $LiNi_{0.5}Co_{0.2}Mn_{0.3}O_2$, especially at high operate voltages (~4.6 V) and high temperatures (~55 ºC) have hindered its widespread application. [14] The chief reason lies in the chemistry that the unstable Ni^{4+} ion in the delithiated $Li_{1-\delta}[Ni_{1-x}M_x]O_2$ materials is readily reduced to Ni^{3+}, which causes a structural transformation to form a more stable rock salt phase ($Li_xNi_{1-x}O$, NaCl structure) and a spinel $Li(Ni_{0.5}Co_{0.2}Mn_{0.3})_2O_4$ phase, [15] resulting in an increase in the interfacial impedance and the cycling instability of the cell. [16, 17] Meanwhile, the structure of the delithiated Ni-rich material becomes thermally unstable due to oxygen release from the structure; and upon contact with organic electrolyte, [18] the highly-active delithiated $Li_{1-\delta}[Ni_{1-x}M_x]O_2$ can oxidatively break down electrolyte molecules; and potentially cause a severe thermal runaway with flame and explosion, resultantly from the interaction between organic electrolyte and highly active delithiated $Li_{1-\delta}[Ni_{1-x}M_x]O_2$. [19]

A conventional method to improve the electrochemical stability and thermal properties of cathode materials for LIBs is surface modification (such as coating) of the materials with metal oxides, metal phosphates and so on. Various inorganic compounds, such as $LiAlO_2$,[20] $LiTiO_2$,[21] Li_2ZrO_3,[22] $Al(OH)_3$, [23] AlF_3, [24] $Ni_3(PO_4)_2$, [17] TiO_2, [25] Bi_2O_3 [26] and $FePO_4$, [27] have been investigated as surface coating agents (usually a thin layer) to improve the cycling performance and thermal stability of cathode materials. The coating layers improve the interface stability between the active material and electrolyte, protecting the active cathode materials from the attack of HF generated in electrolyte during cycling and suppressing further the oxygen loss from the material. [16, 28] Resultantly, the structural integrity, the electrochemical properties especially at high-temperature, and the thermal stability at the highly delithiated state of Ni-rich $Li[Ni_{1-x}M_x]O_2$ cathode material can be much improved.

Lithium ion conductive Li_2TiO_3 is electrochemically inert in a wide voltage range and structurally stable in organic electrolyte. [29] This inert coating layer can prevent the direct contact between the highly active delithiated $Li_{1-\delta}[Ni_{1-x}M_x]O_2$ and the electrolyte, [28] so the electrolyte decomposition by Ni^{4+} and Co^{4+} oxidation is expected to be relieved and the cathode structure corrosion by HF in the electrolyte is expected to be relieved as well.[30] Furthermore, Li^+ diffusion path is three-dimensional in the Li_2TiO_3 and its ionic conductivity could be

increased when doped with aliovalent ions as a result of vacancies formation. [28] In this regard, it is possible that a doped Li_2TiO_3 coating layer is helpful to improve the rate capability as well as the cycling stability of $Li[Ni_{1-x}M_x]O_2$ materials.

In this work, lithium ion conductive Li_2TiO_3 has been used to coat on the surface of Ni-riched $LiNi_{0.5}Co_{0.2}Mn_{0.3}O_2$ cathode material for LIBs. The $LiTi_2O_3$-modified $LiNi_{0.5}Co_{0.2}Mn_{0.3}O_2$ samples were prepared by a two-step reactions that involves an *in situ* hydrolysis of $Ti(SO_4)_2$ onto the surface of the $LiNi_{0.5}Co_{0.2}Mn_{0.3}O_2$ precursor ($[Ni_{0.5}Co_{0.2}Mn_{0.3}](OH)_2$), which could obtain a uniform Li_2TiO_3-precursor (TiO_2) coating, and a subsequent lithiation process with LiOH. In lithiation process, some Ti may enter into the host $LiNi_{0.5}Co_{0.2}Mn_{0.3}O_2$ cathode and trace M (M=Ni, Co, Mn) also could enter into the Li_2TiO_3 phase to formed doped material. The composite materials present excellent cycling stability as well as improved thermal stability, especially at high cut-off voltages and high temperatures. Furthermore, the internal mechanism of LTO effect on NCM is firstly tentatively explored.

Experimental section

Material preparation

The spherical precursor compound $[Ni_{0.5}Co_{0.2}Mn_{0.3}](OH)_2$ was purchased from Ningbo Jinhe New Materials Co., Ltd. After air-drying, 9.16 g $[Ni_{0.5}Co_{0.2}Mn_{0.3}](OH)_2$ powder was put into a baker with 150 ml deionized water under constant stirring at 55 ºC. The caculated $Ti(SO_4)_2$ and NaOH (1:4, n/n) were dissolved in deionized water separately, then the obtained solutions were subsequently injected into the above suspension dropwise The $[Ni_{0.5}Co_{0.2}Mn_{0.3}](OH)_2$ samples coated with 1wt%, 3wt% and 5wt% TiO_2 were denoted as 1% TiO_2@NCMOH, 3% TiO_2@NCMOH and 5% TiO_2@NCMOH, respectively. After filtration, the precursor was washed with distilled water and alcohol for several times. The dried precursor was mixed with appropriate LiOH, then ball-milled at 200 rpm for 1 h (FRITSCH-Pulverisette 14). The ball-milled mixture was first sintered in air atmosphere at 850 ºC for 12 h, then cooled down naturely to room temperature. The $LiNi_{0.5}Co_{0.2}Mn_{0.3}O_2$ samples coated of 1wt%, 3wt% and 5wt% Li_2TiO_3 were denoted as 1% LTO@NCM, 3% LTO@NCM and 5% LTO@NCM, respectively.

Material characterization

The XRD data was collected on Rigaku miniflex 600 with Cu Kα radiation operated at 40 kV and 15 mA scanned from 10º to 90º at 1º min^{-1} with a step size of 0.02º. Field emission scanning electron microscopy (SEM, HITACHI S-4800) was used to characterize the morphology of samples, and energy dispersive X-ray spectroscopy (EDS, OXFORD 7593-H, an accessory of SEM) was carried out to analyze the surface elemental distribution of particles with 20 kV acceleration voltage. Transmission electron microscopy (TEM, JEOL-2100) was used to examine the morphologies and identify the structures of the as-prepared samples. The X-ray photoelectron spectroscopy (XPS) data was collected with a Quantum 2000 Scanning ESCA Microprobe spectrometer with a focused monochromatized Al Kα radiation (1486.6 eV). The pass energies were 60 eV for the survey spectra and 20 eV for particular elements, respectively. The test samples are obtained from clipping the corresponding pasted electrode pole piece without sputtering processing. The DSC/TG (STA 449 F3 Jupiter Netzsch) was used to measure the thermal stability of electrodes from 100 ºC to 400 ºC at a heating rate of 5 ºC /min with an electrolyte of 1 M $LiPF_6$ salt dissolved in ethylene carbonate (EC) and dimethyl carbonate (DMC) with mass ratio of 1:1 (#301 electrolyte, Guotai Huarong, China). The detailed measurements were as follows. Firstly, the button cell was cycled for one cycle and then charged to 4.6 V state. The charged cell was taken apart to get electrode material films in an Ar-filled glove box. The film was washed several times by DMC and naturally dried. The electrode materials scraped from film and electrolyte were sealed together in a gold-plated stainless steel crucible in the glove box. The ratio of electrolyte to electrode materials was 1 μL of electrolyte per milligram of electrode materials.

Electrochemical Measurements.

Electrochemical performances of these materials were evaluated with CR2016-type coin cell configuration. The working electrode film was obtained by spreading a slurry of 85 wt% active material, 8 wt% acetylene black, 2 wt% graphite black and 5 wt% polyvinylidene difluoride (PVDF) binder dispersed in N-methyl pyrrolidione (NMP) solvent onto an aluminum foil. After drying in a vacuum oven at 80 ºC overnight, the electrode was punched out and roll-pressed. CR2016-type coin cells were assembled by sandwiching a porous polyethylene separator between the electrode and Li metal foil in a high-purity Ar-filled glove box. The electrolyte was 1.0 M $LiPF_6$ salt dissolved in a solution of ethylene carbonate (EC) and dimethyl carbonate (DMC) with a weight ratio of 1:1. The mass loading for all the cells was controlled in about 5 $mg \cdot cm^{-2}$.

The cells were charged with constant current and constant voltage mode (CC-CV), and discharged with specific constant current between 3.0-4.6 V at room temperature on battery testers (NEWARE BTS type battery charger, Shenzhen, China). Taking 1 C (170 $mA \cdot g^{-1}$) as an example, the cells were first charged galvanostatically to 4.6 V, after 4.6 V was reached, the voltage was kept at 4.6 V until the current decreases gradually from 1 to 0.1 C (constant voltage charge step). The specific capacity obtained was calculated basing on the composite material mass (Li_2TiO_3 and $LiNi_{0.5}Co_{0.2}Mn_{0.3}O_2$) in the electrode. Cyclic voltammogram (CV) measurements were performed on a CHI 660D potentiostat (Chenghua, Shanghai, China) at a scan rate of 0.1 mV s^{-1} with potential range from 3.1 to 4.6 V. Electrochemical impedance spectra (EIS) were measured at Solartron SI 1287 workstation with a frequency range from 0.005 Hz to 100 kHz. All the tests were conducted at 25 ºC unless specified.

Results and discussion

Fig. 1 shows the SEM images of precursor compounds: $[Ni_{0.5}Co_{0.2}Mn_{0.3}](OH)_2$ (a, b), 1% TiO_2@NCMOH (c, d), 3% TiO_2@NCMOH (e, f) and 5% TiO_2@NCMOH (g, h), respectively. The particles of the precursor $[Ni_{0.5}Co_{0.2}Mn_{0.3}](OH)_2$ are spherical with size ranging from 6 μm to 14 μm. Their surfaces as shown in Fig. 1b are smooth. After the coating with TiO_2, the surfaces of TiO_2@NCMOH become rough with some small nano-particles. At higher loading, for example 5% TiO_2@NCMOH (Fig. 1h), the surface of $[Ni_{0.5}Co_{0.2}Mn_{0.3}](OH)_2$ is fully coated with thick nano-particles layer. EDS spectra of 3% LTO@NCMOH precursor was performed to check the uniformity of the TO_2 coating layer on the surface of coated NCM precursor. It is seen from Fig. 2 that the Ti(e) element distribution is completely overlapped with that of Ni(b), Mn(c) and Co(d) element, indicating that TO_2 is coated on the NCM precursor surface uniformly.

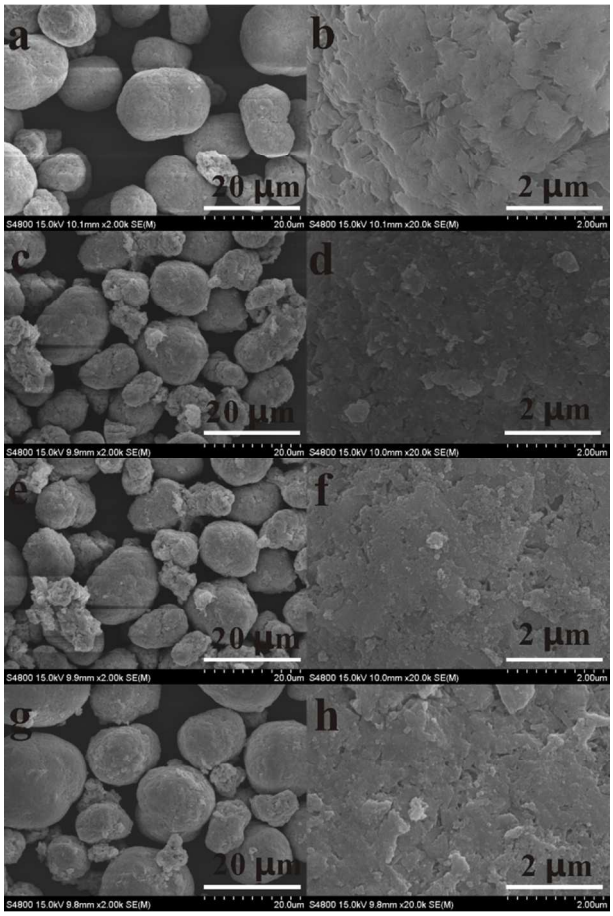

Fig. 1. SEM images of precursor compound $[Ni_{0.5}Co_{0.2}Mn_{0.3}](OH)_2$ (a, b), 1% TiO_2@NCMOH (c, d), 3% TiO_2@NCMOH (e, f) and 5% TiO_2@NCMOH (g, h).

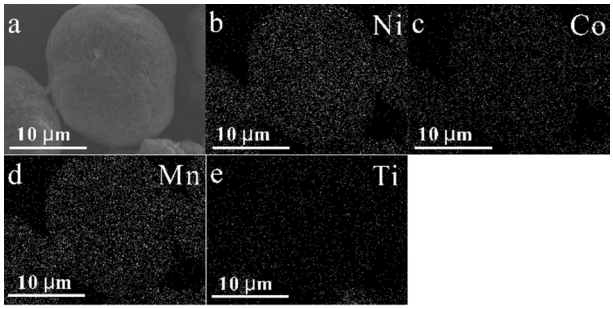

Fig. 2. SEM plot (a) and corresponding EDS area mappings of Ni (b), Co (c), Mn (d) and Ti (e) for 3% TiO_2@NCMOH.

The SEM images of morphologies and microstructures of the NCM, 1% LTO@NCM, 3% LTO@NCM and 5% LTO@NCM composite materials are shown in Fig. 3a-d, respectively, and the corresponding detailed views are shown as insets. Under high-magnification (Fig. 3a insets), it can be seen that the surfaces of NCM microspheres are smooth. The surface morphologies of LTO@NCM samples become fuzzy as the LTO coating content increases.

EDS area mapping analysis of 3% LTO@NCM composite material presented in Fig. 4 was performed to further identify the distribution of the LTO coating layer on the surface of coated NCM. It is seen from Fig. 4b-e that the Ti(e) element distribution is completely overlapped with that of Ni(b), Co(c) and Mn(d) element, suggesting that LTO is cladded on the LNMO surface uniformly.

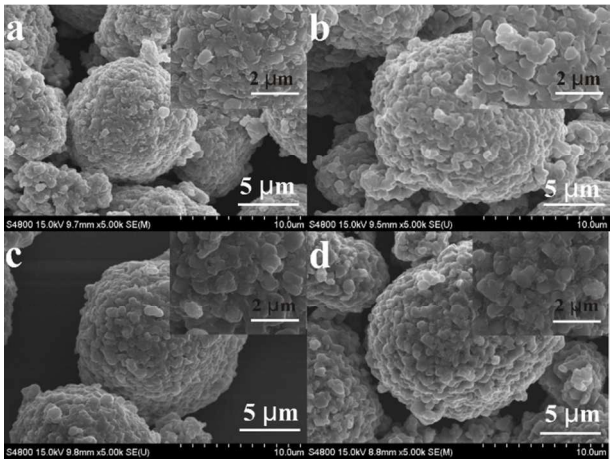

Fig. 3. SEM plots of (a) NCM, (b) 1% LTO@NCM, 3% LTO@NCM and 5% LTO@NCM.

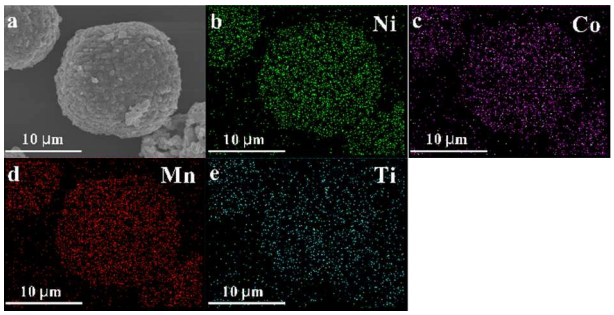

Fig. 4. SEM plot (a) and corresponding EDS area mappings of Ni (b), Co (c), Mn (d) and Ti (e) for 3% LTO@NCM..

To identify the interfacial structure of 3% LTO@NCM particles (which shows best electrochemical performances, shown later), we carried out TEM and surface EDS analyses, as seen in Fig. 5. Fig. 5a and Fig. 5b are high-resolution TEM (HRTEM) images of NCM and 3% LTO@NCM particle, respectively. The surface of NCM is uniform without any coating layer as expected, while in 3% LTO@NCM an obvious coating layer appears with a thickness of cal. 14 nm. A small quantity of Ni^{2+}, Co^{3+} and Mn^{4+} can be doped in Li_2TiO_3 and small amount of Ti^{4+} can be doped in the NCM structure during calcination process. However, this migration ions occupy a small amount of total. Similar phenomenon were also reported by Li's results. [28] The high-resolution TEM (HRTEM) images of 3% LTO@NCM particle shown in Fig. 5c, presents a clear interplanar spacing lattice of 0.48 nm throughout the shell , which is in agreement with the d-spacing of the (002) crystal planes of the monoclinic Li_2TiO_3. [30] This means that the hierarchical LTO is coated successfully on the surface of NCM, as desired. The EDS elemental analysis of selected areas marked d and e region in Fig. 5c are shown in Fig. 5d and Fig. 5e. The Ti atomic content of d region is four times higher than that of e region, suggesting that the surface layer is Ti-rich. The presence of Co, Mn and Ni elements is likely due to the doping of Ni^{2+}, Co^{3+} and Mn^{4+} ions in Li_2TiO_3. This further suggests the coating material is LTO.

Journal Name RSCPublishing

ARTICLE

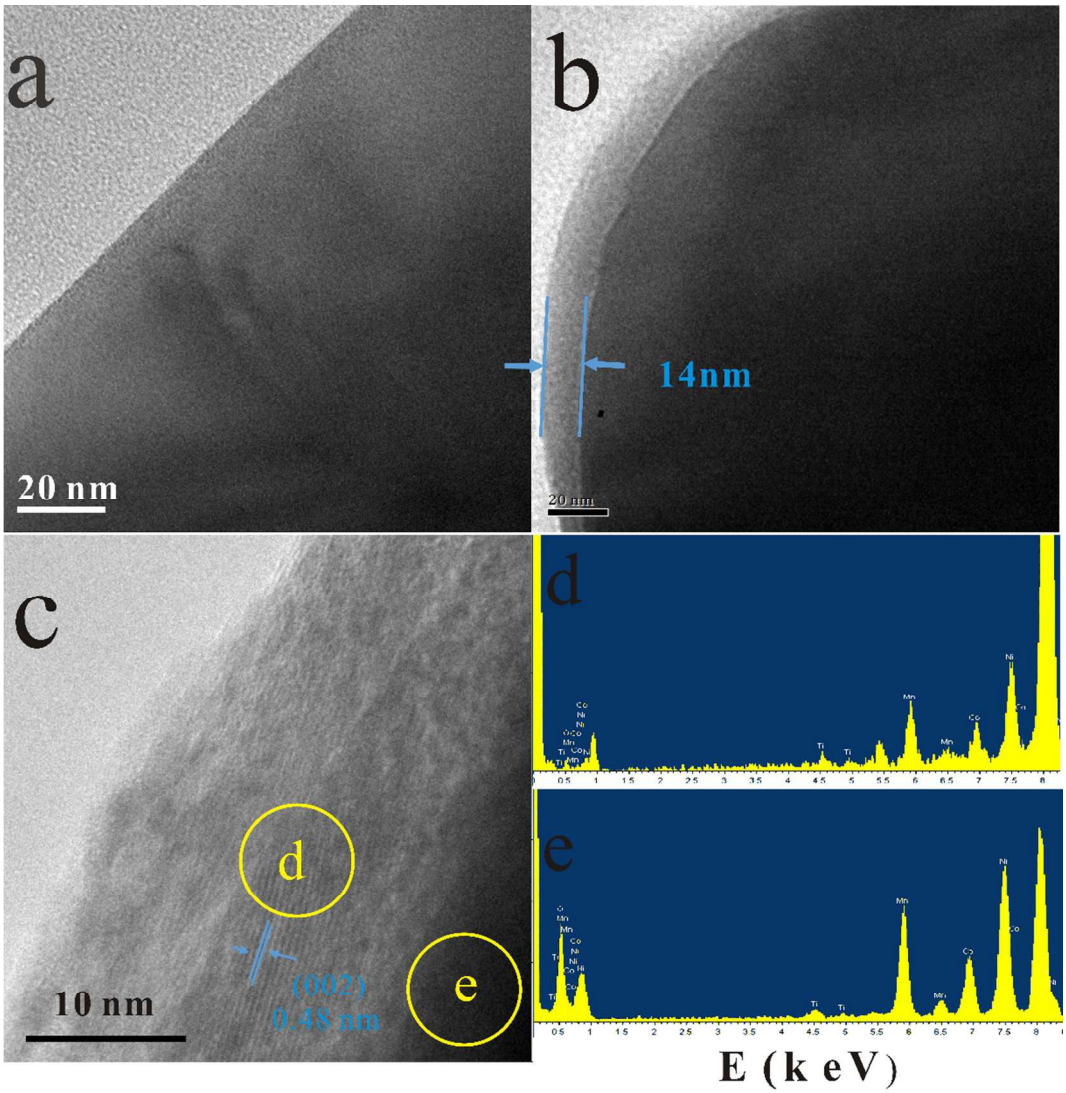

Fig. 5. (a) HR-TEM image of NCM, (b, c) HR-TEM image of 3% LTO@NCM, (d, e) the corresponding surface EDS spectrum of 3% LTO@NCM in the orange area in (c).

In order to further illustrate the Ti distribution, Cross-section SEM image of the 3% LTO@NCM particle and its corresponding EDS were carried out, as shown in Fig. 6. The sample preparation was as following. First, adequate 3% LTO@NCM power were dispersed in a mixture solution of epoxy resin and solidifying agent. Second, the obtained mixture was put in a 60 ºC oven for one day to solidify. Finally, the resultant solid was polished by abrasive paper for metallograph from rough to the subtle to obtain the cross-section of 3% LTO@NCM. Three regions, from the core center to the outer layer (named regions 1–3, respectively), have been chosen to investigate the inner-external composition change of the 3% LTO@NCM. It is noted that the weight ratio of Ni, Co and Mn is close to the stoichiometry and remains almost constant from region 1 to 3, which indicates the bulk of the material is $LiNi_{0.5}Co_{0.2}Mn_{0.3}O_2$. Besides, slight Ti is observed in the core center, and the content of Ti increases slowly from regain 1 to 3, which should be ascribed to diffusion of some Ti during the calcinations process. For regain 3, the content of Ti is increased to 3.2 %, more than quadruple level of that in core. Based on these EDS results, we speculate most Ti ions accumulate on the outer layer of the particle to form LTO, while partial Ti ions enter the bulk $LiNi_{0.5}Co_{0.2}Mn_{0.3}O_2$ with a gradient distribution. Thus, the Ti doped and LTO coated $LiNi_{0.5}Co_{0.2}Mn_{0.3}O_2$ composite is confirmed.

Journal Name RSCPublishing

ARTICLE

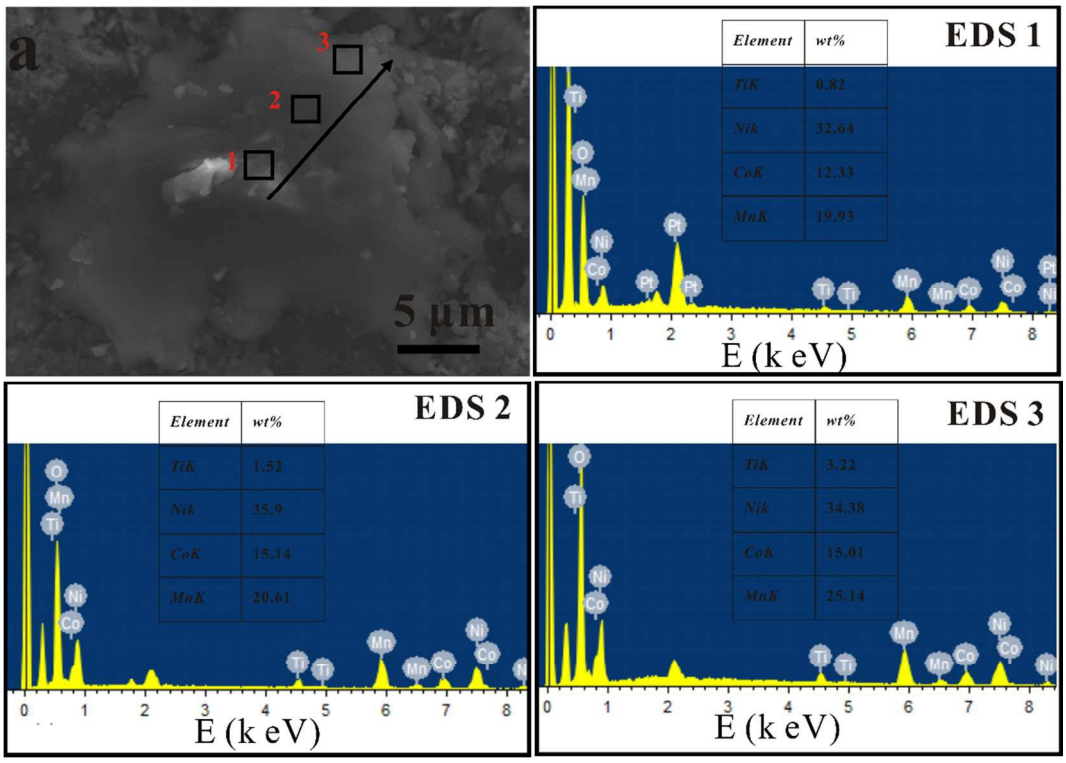

Fig. 6. EDS compositional change from the 3% LTO@NCM particle cross-section.

The XRD patterns of the NCM and LTO@NCM composite are shown in Fig. 7. All the samples exhibit a well-defined layer structure based on a hexagonala-$NaFeO_2$ structure with an $R\bar{3}m$ space group and no impurities present. However, a careful examination of the XRD patterns in a small region between 17 and 20º shows a slight shift to lower angle along with the LTO coating content increases. The lattice parameters, interlayer space of (003) lattice plane, and the integrated intensity ratios of (003)/(104) obtained from the least square refinement based on a cubic structure by the PDXL2 software (Rigaku, Japan), are summarized in Table 1. As seen from the Table 1, both the crystal lattice parameter and interlayer space of (003) lattice plane of the samples increase with the LTO coating content improves, which is attributed to the substitution by some larger Ti^{4+} (0.605 Å) ions for smaller Co^{3+} (0.545 Å) ions and/or Mn^{4+} (0.53 Å) ions in the layered $LiNi_{0.5}Co_{0.3}Mn_{0.2}O_2$ structure. The cation distribution in the lattice of the layered oxide is manifested by intensity ratio of I(003)/I(104). If the intensity ratio of the I(003)/I(104) is lower than 1.2, a high degree of cation mixing is present, due to the occupancy of foreign ions in the lithium region. [31-35] It is noted that the intensity ratio of I(003)/I(104) are all bigger than 1.2, indicating that low cation mixing occurred. ICP-AES was executed to identify the exact content of LTO in composite material. The measured LTO values in 1% LTO@NCM, 3% LTO@NCM and 5% LTO@NCM are 0.87%, 2.82% and 4.8%, respectively, in a good agreements with those designed values.

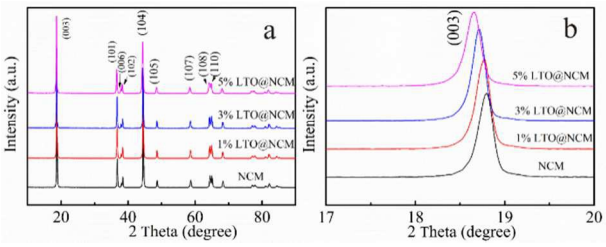

Fig. 7. (a) XRD plots of samples, (b) magnifying graphs of (a) in specific zone.

In order to observe the oxidation state of transition metals at the surface of 3% LTO@NCM, XPS test is performed, and the corresponding spectra are depicted in Fig. 8. All of the binding energies are revised using C 1s peak (set at 284.6 eV) as reference.

Table 1 The summary of lattice parameters for all samples, d_{003}, and the integrated intensity ratios of the (003)/(104) for the as-synthesized samples.

Samples	a-Axis (Å)	c-Axis (Å)	c/ a	d (003) (Å)	$I_{(003)}/I_{(104)}$
NCM	2.869	14.206	4.951	4.717	1.320
1%LTO@NCM	2.869	14.213	4.954	4.723	1.337
3%LTO@NCM	2.870	14.234	4.960	4.737	1.289
5%LTO@NCM	2.878	14.262	4.956	4.752	1.394

The binding energies of Ni $2p_{3/2}$/Ni $2p_{1/2}$, Co $2p_{3/2}$/Co $2p_{1/2}$ and Mn $2p_{3/2}$/Mn $2p_{1/2}$ on the surface of 3% LTO@NCM material are 854.3 eV/871.9 eV, 780.2 eV/795.4 eV and 642.5 eV/653.8 eV, which are consistent with the metal ions valences of Ni^{2+}, Co^{3+}, Mn^{4+}, respectively. These results are consisted with previous XPS results for NCM [36], further indicating that coating modifications don't change the basic structure of NCM. Meanwhile, the Ti $2p_{3/2}$ and Ti $2p_{1/2}$ peaks of

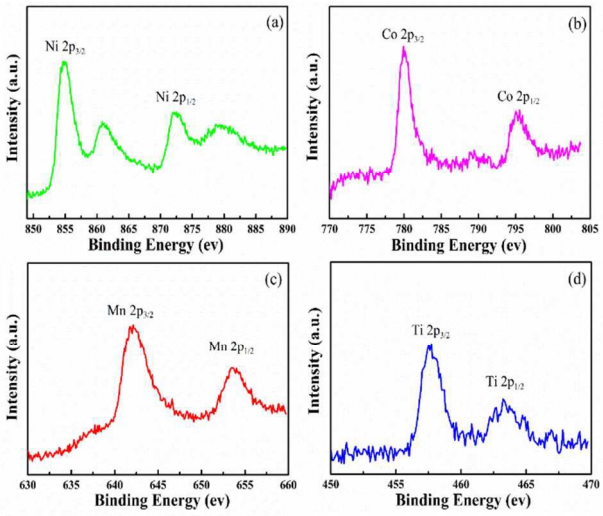

Fig. 8 XPS profiles of (a) Ni, (b) Co, (c) Mn, and (d) Ti on the surface of the 3% LTO@NCM composite material.

3% LTO@NCM shown in Fig. 8d are located at 457.8 eV and 463.3 eV, in accordance with Ti^{4+} oxidation state of the Li_2TiO_3 material. [30] This further indirectly proves that the surface coating material of LTO@NCM is Li_2TiO_3.

The electrochemical behaviors of the samples without and with LTO coating were investigated by CV tests, conducted at a scanning rate of 0.1 mV s^{-1} at 25 ºC, and depicted in Fig. 9. The intense and sharp reduction/oxidation peaks of Ni^{2+}/Ni^{4+} are observed at around 3.8 V in both NCM and 3% LTO@NCM samples. After the first cycle, the oxidization peak of NCM shifts from 3.97 V to 3.86 V, while that of 3% LTO@NCM from 3.93 V to 3.87 V. The smaller difference in the oxidization peak position of 3% LTO@NCM between first and second cycle means less polarization because LTO suppress the side reaction between electrolyte and NCM. The oxidation and reduction peaks of 3% LTO@NCM are sharper and the shift of corresponding peaks between the first and the second cycles is smaller compared with that of NCM, meaning 3% LTO@NCM has an better electrochemical reversibility and faster lithium insertion/extraction. [37] The reduction peak of NCM at 100th shifts to lower potential than that of 3% LTO@NCM due to further polarization in NCM.

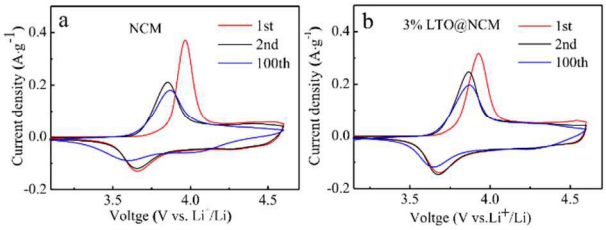

Fig. 9. CVs plots at 25 ºC with a scanning speed of 0.1mV s^{-1}: (a) NCM, (b) 3% LTO@NCM.

The initial discharge curves of the samples NCM, 1% LTO@NCM, 3% LTO@NCM and 5% LTO@NCM are plotted in Fig. 10 over the voltage range of 3-4.6 V at 0.2 C (34 mA g^{-1}) at room temperature. After LTO coating, the plateaus corresponding to Li^+ ions extraction/insertion from/into the 3a sites don't change obviously, again indicating LTO-coating doesn't change the basic structure of NCM (consistent with XRD results). The discharge capacities of NCM, 1% LTO@NCM, 3% LTO@NCM and 5% LTO@NCM are 187.8 mAh g^{-1}, 186.2 mAh g^{-1}, 182.2 mAh g^{-1} and 179.2 mAh g^{-1}, respectively. The small declines of discharge capacities along with the increase of coating contents are attributed to the calculated mass basing on the composite material mass (Li_2TiO_3 and $LiNi_{0.5}Co_{0.2}Mn_{0.3}O_2$) in the electrodes.

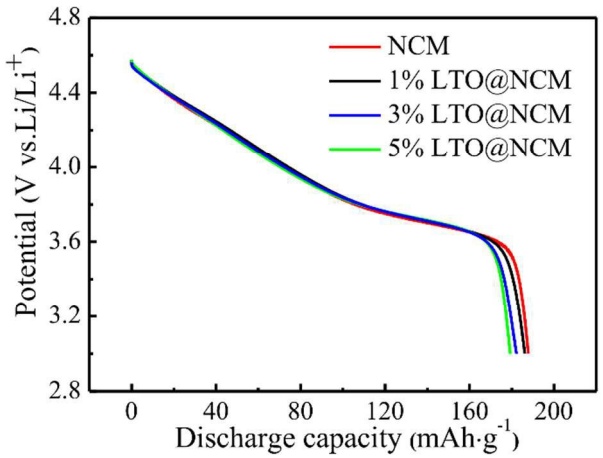

Fig. 10. First discharge profiles of samples at 0.2 C

The subsequent discharge cycle profiles at 1 C charge rate and 1 C discharge rate of the samples NCM, 1% LTO@NCM, 3% LTO@NCM and 5% LTO@NCM are shown in Fig. 11. Their first discharge capacities are 182.8, 181.8, 178.0 and 172.0 mAh·g^{-1}, respectively. After 100 cycles, the discharge capacities decrease steadily to 136.4, 150.6, 164.5 and 147.0 mAh·g^{-1}, which is equal to 74.3%, 82.8%, 92.4% and 85.4% of their first capacities, respectively. The capacity retention of the 3% LTO@NCM is the highest, while that of the 5% LTO@NCM is relative low. This may be ascribed to poor electric conductivity of LTO. So, appropriate coating is beneficial, and thicker coating layer increases the resistance for electron transportation among particles that is responsible for the lower discharge capacity of 5% LTO@NCM.

Fig. 11(b) shows the rate performance of the NCM and 3% LTO@NCM cathode material ranging from 0.2 C to 10 C. The discharge capacities of NCM at 0.2 C, 0.5 C, 1 C, 2 C, 5 C and 10 C are 180.0 mAh g^{-1}, 165.5 mAh·g^{-1}, 149.9 mAh g^{-1}, 131.7 mAh g^{-1}, 99.2 mAh g^{-1} and 43.8 mAh g^{-1}, respectively. When the current value is returned back to 0.2 C, a reversible discharge capacity of 170.4 mAh g^{-1} is obtained, which is 90.7% of the initial discharge capacity at the same rate. After coating of 3% LTO, the specific discharge capacities are 180.1, 174.6, 168.4, 157.4, 136.5 and 108.2 mAh·g^{-1} at the rates of 0.2, 0.5, 1, 2, 5 and 10 C, respectively. As the current is back to 0.2 C, the discharge capacity returns to 174.4 mAh·g^{-1}, which is 96.8% capacity retention of the initial discharge capacity at 0.2 C. The capacity of 3% LTO@NCM at 10 C is even higher than that of NCM at 5 C. Thus LTO coating facilitates Li ion transportation and stabilizes the NCM structure.

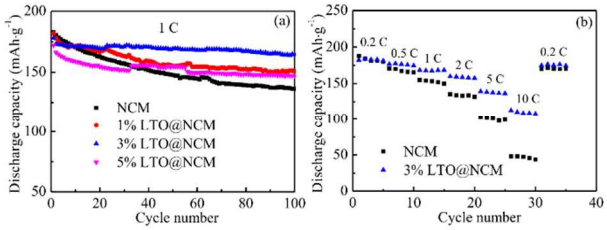

Fig. 11. Electrochemical properties of the as prepared samples: (a) cycle performance at 1 C, (b) rate cycling performance of the samples.

Electrochemical impedance spectroscopy was carried out to further illustrate the difference between NCM and 3% LTO@NCM regarding electrochemical polarization and ohmic polarization, as shown in Fig. 12. All the cells were charged at 1 C by constant current and constant potential process, and discharged via constant current process for 20 and 60 cycles, and then the cathode was charged to 4.6 V. The EIS tests were measured in the range from 100 kHz to 0.005 Hz. The Nyquist plots of both materials display similar profiles with two semicircles in the high-frequency region, and their equivalent circuits are the same as shown in Fig. 12 insets. In the equivalent circuit, the R_1 is ascribed to electrolyte resistance, while the R_2 is attributed to the cathode surface film (similar to anode SEI layer) and direct charge transfer resistance of electrode materials and R_3 is assigned to resistance of the anode. CPEs present the double layer capacitance or passivation film capacitance. Wo represents the Warburg impedance. [38, 39] The solid line is the fitted results of measured data (dotted value). It is clearly seen that the equivalent circuit model is adequate for the fitting as the dotted and solid lines are overlapping. The fitted values of these components are listed in Table 2. Obviously, the LTO-coating NCM electrode exhibits a much smaller charge-transfer resistance than that of the pristine NCM electrode, indicating that LTO modification of the NCM material is favourable for lithium ion mobility. The R_2 values of 3% LTO@NCM at 20th is 24.8, while that of NCM is 30.4 Ω. The R_2 and R_3 of 3% LTO@NCM cathode at 60th don't change much compared with those of 20th. However, the R_2 and R_3 of NCM cathode at 60th increased by half compared with those of 20th. According to previous literature reports, Ni^{4+} ions formed at the deintercalation state of the cathode ($Li_{1-x}Ni_{0.5}Co_{0.2}Mn_{0.3}O_2$) are reactive toward liquid electrolyte and can catalyze the oxidation of the electrolyte, triggering the oxygen loss from the surface of the material, accompanied by a phase transformation from rhombohedral phase to a mix of spinel and rock salt phases, which is the major reason for the capacity fading of NCM during the cycle performance. [15] Based upon the better cycling presented in this work, it is obvious the LTO can serve as a protective layer to inhibits the electrolyte decomposition at the electrode/electrolyte interface and thereby lower interface charge transfer resistance, and improves the structure integrity and its capacity retention during long-term charge–discharge cycles.

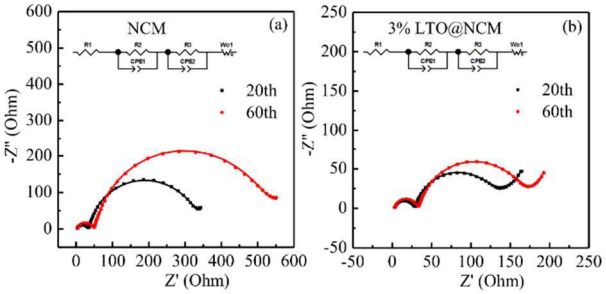

Fig. 12. EIS spectra of the samples in the frequency range between 0.005 Hz and 100 kHz at 25 ºC. The insets show the equivalent circuits for the EIS measurements.

Table 2. Impedance parameter of electrodes.

	R1(Ω)	R2(Ω)	R3(Ω)
NCM (20th)	2.1	30.4	272.0
NCM (60th)	2.8	44.6	438.7
3% LTO@NCM (20th)	3.1	24.8	86.6
3% LTO@NCM (60th)	3.1	28.3	114.9

CV scanning was performed to further explain the different electrochemical behaviors of the samples. The cells were charged and discharged at the rate of C/20 for one cycle prior to the CV scanning. Fig. 13 shows the CV plots of NCM and 3% LTO@NCM samples at various scan rates from 0.2 to 1 mV·s^{-1}. As seen in Fig. 13, the peak current density is proportional to the square root of the scanning rate, indicating that the electrode reaction is a reversible process. For a reversible reaction, the peak current density during oxidative-reductive scans at different rates can be used to calculate the Li^+ diffusion coefficient (D_{Li}) using the Randles–Sevcik equation [40]:

$$i_p/m = 0.4463n^{3/2}F^{3/2}C_{Li}A_eR^{-1/2}T^{-1/2}D_{Li}^{1/2}\upsilon^{1/2} \quad (1)$$

where n, F, C_{Li}, A_e, R, T, and υ are the number of electrons per molecule during redox process, the Faraday's constant, the concentration of lithium ion, the surface area, the gas constant, the absolute temperature and the scanning rate, respectively. Fig. 13 c-d present the i_p/m-$\upsilon^{1/2}$ plots, the relationship between the i_p/m and $\upsilon^{1/2}$ is linear. According to Eq. (1), the Li^+ coefficients of NMO and 3% LTO@NCM are calculated to be approximate 5.57×10^{-11} and 1.68×10^{-10} $cm^2 \cdot s^{-1}$, respectively. Clearly, the Li^+ diffusion coefficient is greatly improved due to the LTO coating.

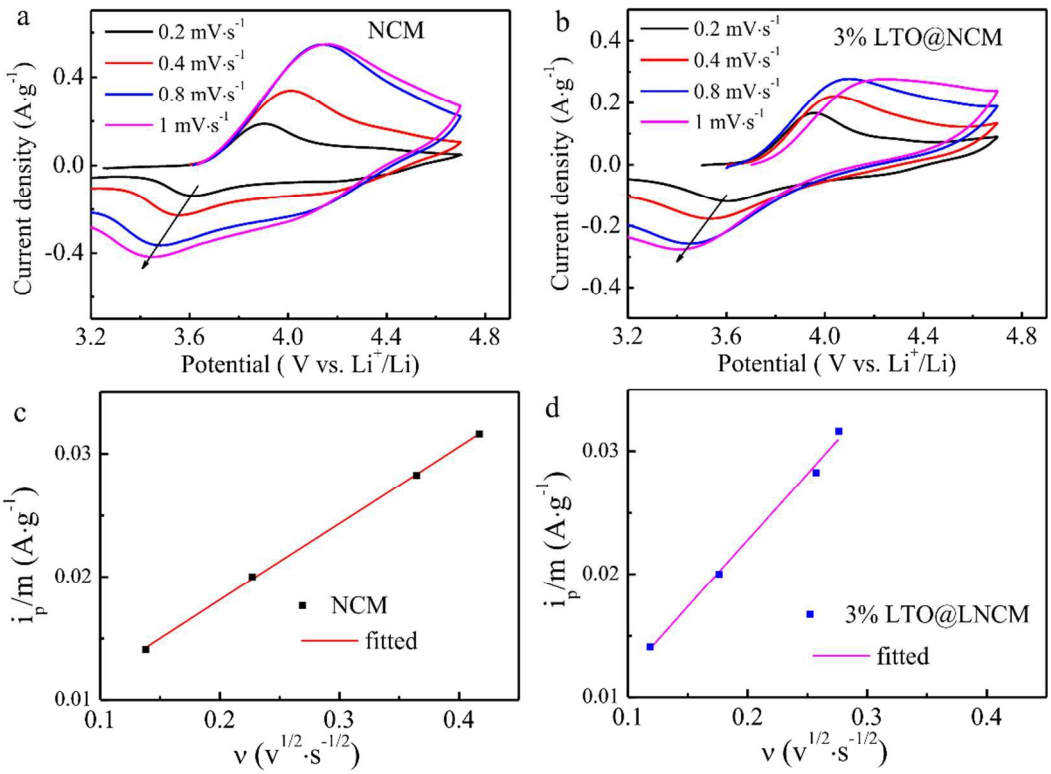

Fig. 13. CV plots of (a) NCM and (b) 3% LTO@NCM at different scan rates; and the plots of reductive peak current density (I_P) as a function of the square root of the scan rate ($v^{1/2}$) for (c) NCM and (d) 3% LTO@NCM.

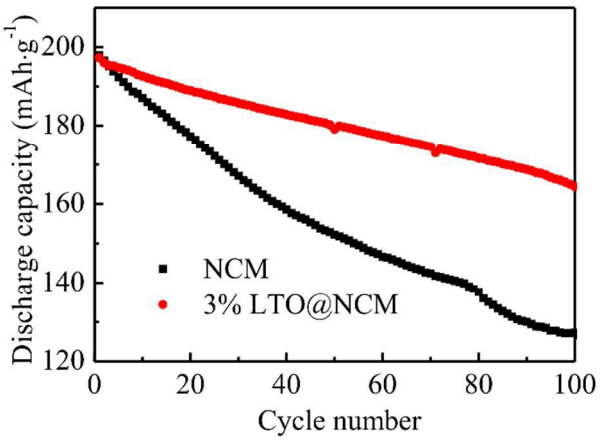

Fig. 14. Cycle performance of NCM and 3% LTO@NCM at 1 C at 55 ºC

Fig. 14 shows cycle performance of NCM and 3% LTO@NCM electrodes at 55 ºC at 1 C rate. The NCM and 3% LTO@NCM materials exhibit specific discharge capacities of 198.0 and 197.3 $mAh \cdot g^{-1}$ at first cycle, respectively. The obvious difference is that the capacity of NCM faded quickly, with capacity retention of 63.9% after 100 cycles, whereas the capacity of 3% LTO@NCM faded gradually and was 83.7% of the initial capacity after 100 cycles. From these results, we believe that LTO coating layer can form a stable barrier between NCM and electrolyte at elevated temperature to prevent the side reactions between them therefore to enhance the electrode performance at high-temperature.

Table 3 presents the concentrations of Ni, Co and Mn cations of NCM and 3% LTO@NMO dissolved in the electrolyte. The cell was charged to fully delithiated state at 0.2 C, then unpacked to obtain electrode materials film in an Ar-filled glove box. The electrode film was immersed in 301 electrolyte with the ratio of electrode materials to electrolyte was 2 mg to 1 ml at 80 ºC for 12 h. After acid-treating to remove organics, the storage electrolyte was carried out for metal ion test by ICP instrument. The concentrations of Ni and Co, especially for Mn cations of 3% LTO@NCM dissolved in the electrolyte are lower than those of NCM, which suggests that the LTO coating layer successfully alleviated the dissolution of transition metals and stabilized NCM structure. This LTO protective coating suppressed HF scavenger of NCM in electrolyte, leading to enhanced electrochemical properties.

Table 3 The concentration of Ni, Co and Mn cations dissolved in the electrolyte for NCM and 3% LTO@NCM electrodes stored at 80 ºC for 12 h.

	Ni (ppm)	Co (ppm)	Mn (ppm)
NCM	7.08	2.58	6.06
3% LTO@NCM	5.67	2.20	4.50

To examine structural stability of NCM and 3% LTO@NCM, *ex situ* XRD study of electrode were performed before and after charge-discharge process at 25 ºC and at 55 ºC, as shown in Fig 15

(black lines are electrodes before cycle, red lines are after 100 cycle at 25 °C and green lines are after 100 cycle at 55 °C). The samples were cycled for 100 cycles at 1 C before the XRD measurements. When cycled at 25 ºC, the structures of NCM and 3% LTO@NCM don't change much, and peak positions don't changed. However, when cycled at 55 ºC, the (006) peak of NCM shifted toward smaller 2θ moving close to (101) peak and a new peak around 65.7 ° emerged, which are all attributed to Li deficient spinel $Li(Ni_{0.5}Co_{0.2}Mn_{0.3})_2O_4$ phase. On the other hand, in the case of 3% LTO@NCM, (006) peak doesn't change and new peak is absent, implying the more stable structure of NCM after LTO-coating. The new peak around 25.7 º appeared in both NCM and 3% LTO@NCM when cycled at 55 ºC may be ascribed to Li_2NiO_2 phase. At room temperature, the spinel phase transform and side reaction of layered structure are not obvious, so the XRD patterns before and after cycle are the same. [15] While at high temperature, oxygen evolution in Ni-based layered structures is severe accompanied by a structural transformation from layered $LiMO_2$ into a spinel structure. [11] Nevertheless, LTO coating successfully suppress the oxygen loss from the surface of the material, consequently the structure of NCM become more stable. This is also the reason that the electrochemical property and rate capacity of 3% LTO@NCM are superior to those of pristine NCM.

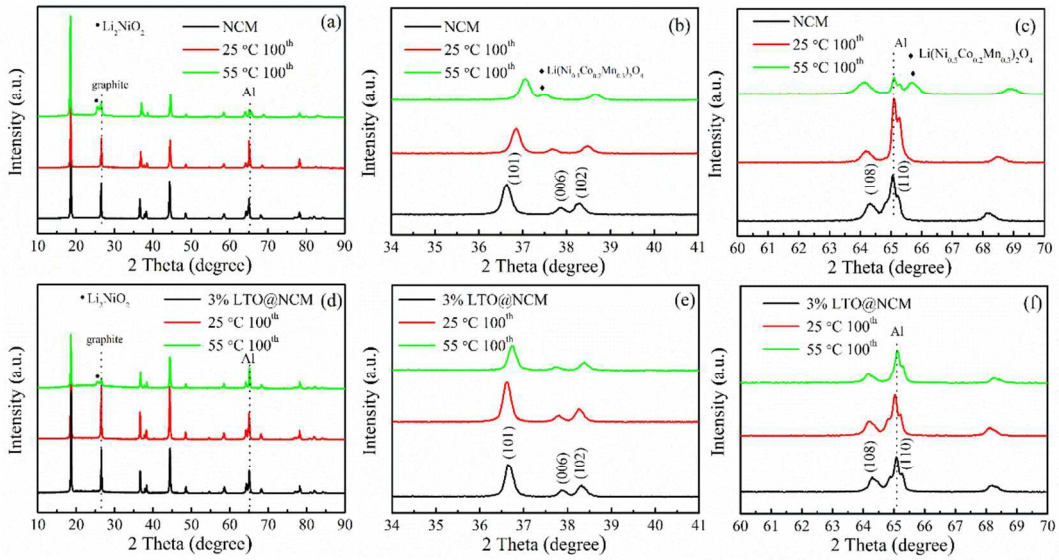

Fig. 15. Ex situ XRD patterns of NCM (a-c) and 3% LTO@NCM (d-f): before cycle (black line), after 100 cycle at 25 °C (red line) and after 100 cycle at 55 °C (green line).

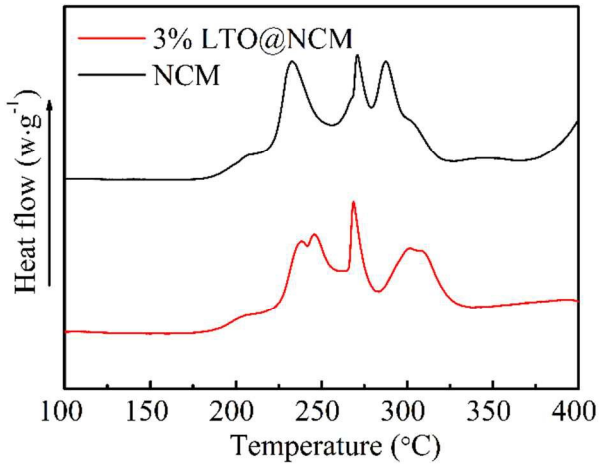

Fig. 16. DSC curves of samples in #301 electrolyte at the states of charged to 4.6 V.

The thermal behaviors of charged (delithiated, 4.6 V) NCM and 3% LTO@ NCM in 301 electrolyte (1M $LiPF_6$, EC/DMC) were investigated by DSC/TG analysis as shown in Fig. 16. The onset exothermic temperatures for these two samples are both at *cal.* 181.2 ºC, however the total heat quantity for 3% LTO@NCM around 180-350 ºC is 1478 $J \cdot g^{-1}$, while that of NCM is 1764 $J \cdot g^{-1}$. The third exothermic peak of NCM is moved from 287.3 ºC to 305.3 ºC after 3% LTO coating. LTO working as a protective layer observably inhibits the interaction between NCM and the electrolyte, and suppresses the electrolyte decomposition at the electrode/electrolyte interface, therefore improves the thermostability of NCM.

Conclusions

In summary, we developed a simple and commercially feasible method to modify the NCM surface with LTO coating. Structural characterizations by SEM, XRD and TEM show that the coating is uniform, and the structure of NCM is retained. The electrochemical tests demonstrate that LTO coating improve NCM electrochemical performance. The coating content of LTO up to 3% in the NCM exhibits the excellent electrochemical cycle, presenting a discharge specific capacity of 178.0 $mAh \cdot g^{-1}$ at 1 C with a retention of 92.4% after 100 cycles. In addition, it also shows remarkable rate capability, the discharge specific capacity decreased slightly from 180.1 to 174.6, 168.4, 157.4, 136.5 and 108.2 $mAh \cdot g^{-1}$ at 0.2 C, 0.5 C, 1 C, 2 C, 5 C and 10 C, respectively. Furthermore, it has superior electrochemical property at elevated temperature and high rates. At 1 C rate at 55 ºC, the discharge capacity of 3% LTO@NCM is up to 197.3 $mAh \cdot g^{-1}$, with a retention of 83.4% after 100 cycles. Also, phase transformation of NCM at high-temperature and metal ions are effectively suppressed after LTO-coating. These results illustrate that LTO coating can work as an isolating layer to inhibit the interaction

between NCM cathode and the electrolyte, alleviate the dissolution of metal ions and phase transformation in NCM, and improve its structural stability.

Acknowledgments

The authors gratefully acknowledge the financial supports from the National High Technology Research and Development Program of China (2012AA110204), Key Project of Science and Technology of Fujian Province (2013H6022), Science and Technology Bureau of Xiamen (Grant No. 3502Z20133004), National Natural Science Foundation of China (21321062) and National Found for Fostering Talents of Basic Science (J1310024). The authors also wish to express their thanks to Drs. Dong Sun and Binbin Xu for their valuable suggestions

Notes and references

[a] State Key Lab of Physical Chemistry of Solid Surfaces, Department of Chemistry, Collaborative Innovation Center of Chemistry for Energy Materials, College of Chemistry and Chemical Engineering, Xiamen University, Xiamen, 361005, P. R. China.

[b] School of Energy Research, Xiamen University, Xiamen, 361005,P.R. China.

E-mail: jbzhao@xmu.edu.cn

1. W. Yang, X. Liu, Y. J. Wang, B. Barbiellini, H. Hafiz, S. Basak, J. Liu, T. Richardson, F.-C. Chou, G.-J. Shu, T.-C. Weng, D. Nordlund, D. Sokaras, T. Deveraux, B. Moritz, R. Qiao, Y.-D. Chuang, A. Bansil and Z. Hussain, *Phys. Chem. Chem. Phys.*, 2015.
2. X. Feng, Z. Z. Yang, D. C. Tang, Q. Y. Kong, L. Gu, Z. X. Wang and L. Q. Chen, *Phys. Chem. Chem. Phys.*, 2015, **17**, 1257-1264.
3. J. Wang, W. Lin, B. Wu and J. Zhao, *J. Mater Chem. A*, 2014, **2**, 16434-16442.
4. J. Wang, Y. Yu, B. Wu, W. Lin, J. Li and J. Zhao, *J. Mater Chem. A*, 2014.
5. B. Li, Y. Yu and J. Zhao, *J. Power Sources*, 2015, **275**, 64-72.
6. J. B. Goodenough and K.-S. Park, *J. Am. Chem. Soc.*, 2013, **135**, 1167–1176.
7. T. Ohzuku and R. J. Brodd, *J. Power Sources*, 2007, **174**, 449-456.
8. O. K. Park, Y. Cho, S. Lee, H. C. Yoo, H. K. Song and J. Cho, *Energy Environ. Sci.*, 2011, **4**, 1621-1633.
9. B. Scrosati and J. Garche, *J. Power Sources*, 2010, **195**, 2419-2430.
10. X. Xiong, Z. Wang, H. Guo, Q. Zhang and X. Li, *J. Mater Chem. A*, 2013, **1**, 1284-1288.
11. M. Jo, M. Noh, P. Oh, Y. Kim and J. Cho, *Adv. Energy Mater.*, 2014, **4**, 1301583-1301590.
12. M. Zou, M. Yoshio, S. Gopukumar and J.-i. Yamaki, *Chem. Mater.*, 2003, **15**, 4699-4702.
13. Y. Kim, *Phys. Chem. Chem. Phys.*, 2013, **15**, 6400-6405.
14. X. Yang, X. Wang, L. Hu, G. Zou, S. Su, Y. Bai, H. Shu, Q. Wei, B. Hu, L. Ge, D. Wang and L. Liu, *J. Power Sources*, 2013, **242**, 589-596.
15. S.-K. Jung, H. Gwon, J. Hong, K.-Y. Park, D.-H. Seo, H. Kim, J. Hyun, W. Yang and K. Kang, *Adv. Energy Mater.*, 2014, **4**, 1300787-1300794.
16. Y.-K. Sun, B.-R. Lee, H.-J. Noh, H. Wu, S.-T. Myung and K. Amine, *J. Mater Chem.*, 2011, **21**, 10108-10112.
17. D.-J. Lee, B. Scrosati and Y.-K. Sun, *J. Power Sources*, 2011, **196**, 7742-7746.
18. D. W. Shin, C. A. Bridges, A. Huq, M. P. Paranthaman and A. Manthiram, *Chem. Mater.*, 2012, **24**, 3720-3731.
19. Y.-K. Sun, S.-T. Myung, M.-H. Kim, J. Prakash and K. Amine, *J. Am. Chem. Soc.*, 2005, **127**, 13411-13418.
20. L. Li, Z. Chen, Q. Zhang, M. Xu, X. Zhou, H. Zhu and K. Zhang, *J. Mater Chem. A*, 2015, **3**, 894-904.
21. L. Li, Z. Chen, L. Song, M. Xu, H. Zhu, L. Gong and K. Zhang, *J. Alloys Compd.*, 2015, **638**, 77-82.
22. J. Zhang, Z. Li, R. Gao, Z. Hu and X. Liu, *J. Phys. Chem. C*, 2015.
23. S. B. Jang, S. H. Kang, K. Amine, Y. C. Bae and Y. K. Sun, *Electrochim. Acta*, 2005, **50**, 4168-4173.
24. H. B. Kim, B. C. Park, S. T. Myung, K. Amine, J. Prakash and Y. K. Sun, *J. Power Sources*, 2008, **179**, 347-350.
25. W. Liu, M. Wang, X. l. Gao, W. Zhang, J. Chen, H. Zhou and X. Zhang, *J. Alloys Compd.*, 2012, **543**, 181-188.
26. J. Liu and A. Manthiram, *Chem. Mater.*, 2009, **21**, 1695-1707.
27. Y. Bai, X. Wang, S. Yang, X. Zhang, X. Yang, H. Shu and Q. Wu, *J. Alloys Compd.*, 2012, **541**, 125-131.
28. J. Lu, Q. Peng, W. Wang, C. Nan, L. Li and Y. Li, *J. Am. Chem. Soc.*, 2013, **135**, 1649-1652.
29. H. Deng, P. Nie, H. Luo, Y. Zhang, J. Wang and X. Zhang, *J. Mater. Chem. A*, 2014, **2**, 18256-18262.
30. X. Yang, R. Yu, L. Ge, D. Wang, Q. Zhao, X. Wang, Y. Bai, H. Yuan and H. Shu, *J. Mater Chem. A*, 2014, **2**, 8362.
31. J. Li, R. Yao and C. Cao, *ACS Appl. Mater. Interfaces*, 2014, **6**, 5075-5082.
32. C. Nithya, R. Thirunakaran, A. Sivashanmugam and S. Gopukumar, *ACS Appl. Mater. Interfaces*, 2012, **4**, 4040-4046.
33. M. Wang, Y. Chen, F. Wu, Y. Su, L. Chen and D. Wang, *Electrochim. Acta*, 2010, **55**, 8815-8820.
34. Y.-M. Choi, S.-I. Pyun and S.-I. Moon, *Solid State Ionics*, 1996, **89**, 43-52.
35. L. Liang, K. Du, Z. Peng, Y. Cao, J. Duan, J. Jiang and G. Hu, *Electrochim. Acta*, 2014, **130**, 82-89.
36. Y.-M. Lee, K.-M. Nam, E.-H. Hwang, Y.-G. Kwon, D.-H. Kang, S.-S. Kim and S.-W. Song, *J. Phys. Chem. C*, 2014, **118**, 10631-10639.
37. Y. Zhu and C. Wang, *J. Phys. Chem. C*, 2010, **115**, 823-832.
38. L. J. Xi, H.-E. Wang, Z. G. Lu, S. L. Yang, R. G. Ma, J. Q. Deng and C. Y. Chung, *J. Power Sources*, 2012, **198**, 251-257.
39. S. J. Shi, J. P. Tu, Y. Y. Tang, X. Y. Liu, Y. Q. Zhang, X. L. Wang and C. D. Gu, *Electrochim. Acta*, 2013, **88**, 671-679.
40. H. Guo, C. Wu, J. Xie, S. Zhang, G. Cao and X. Zhao, *J. Mater Chem. A*, 2014.

